Magnetic Resonance in Medicine 69:179–187 (2013)

In Vivo CEST MR Imaging of U87 Mice Brain Tumor Angiogenesis Using Targeted LipoCEST Contrast Agent at 7 T

Julien Flament,[1] Françoise Geffroy,[1] Christelle Medina,[2] Caroline Robic,[2] Jean-François Mayer,[2] Sébastien Mériaux,[1] Julien Valette,[1] Philippe Robert,[2] Marc Port,[2] Denis Le Bihan,[1] Franck Lethimonnier,[1] and Fawzi Boumezbeur[1]*

LipoCEST are liposome-encapsulating paramagnetic contrast agents (CA) based on chemical exchange saturation transfer with applications in biomolecular MRI. Their attractive features include biocompatibility, subnanomolar sensitivity, and amenability to functionalization for targeting biomarkers. We demonstrate MR imaging using a targeted lipoCEST, injected intravenously. A lipoCEST carrying Tm(III)-complexes was conjugated to RGD tripeptide (RGD-lipoCEST), to target integrin $\alpha_v\beta_3$ receptors involved in tumor angiogenesis and was compared with an unconjugated lipoCEST. Brain tumors were induced in athymic nude mice by intracerebral injection of U87MG cells and were imaged at 7 T after intravenous injection of either of the two contrast agents (n = 12 for each group). Chemical exchange saturation transfer-MSME sequence was applied over 2 h with an average acquisition time interval of 13.5 min. The chemical exchange saturation transfer signal was ~1% in the tumor and controlateral regions, and decreased to ~0.3% after 2 h; while RGD-lipoCEST signal was ~1.4% in the tumor region and persisted for up to 2 h. Immunohistochemical staining revealed a persistent colocalization of RGD-lipoCEST with $\alpha_v\beta_3$ receptors in the tumor region. These results constitute an encouraging step toward in vivo MRI imaging of tumor angiogenesis using intravenously injected lipoCEST. **Magn Reson Med 69:179–187, 2013.**

Key words: molecular MRI; CEST; lipoCEST contrast agents; tumor angiogenesis; $\alpha_v\beta_3$ imaging; U87MG

During the past few years, several contrast agents (CA) applicable to novel magnetic resonance imaging (MRI) techniques have been developed, in particular for use in imaging by chemical exchange saturation transfer (CEST). Latter is a MRI modality proposed by Balaban et al. (1) that allows an ON/OFF contrast. Recently, a new class of paramagnetic CEST CA, called lipoCEST, have been proposed for molecular MRI by Aime et al. (2) and Guerbet (3). These CAs are nanosized, liposomes filled with a high concentration of paramagnetic shifting complexes. The presence of the lipid bilayer confers a high biocompatibility and the possibility of functionalization by grafting peptides on the outer membrane to target specific biomarkers. The lipoCEST exhibit a much lower shifting power than paraCEST complexes; the maximum reported shift for lipoCEST is −45 ppm (4), whereas paraCEST exhibit a shift as large as −720 ppm (5). However, the shift of bound water protons is large enough to limit the loss in sensitivity due to inherent magnetization transfer (MT) in lipoCEST (6). The main advantages of lipoCEST over paraCEST are their nanomolar sensitivity and their slowed down water exchange rates that allow for an efficient chemical saturation at lower saturation power (7). These properties make lipoCEST a very promising tool for applications in medical and biological fields.

Basically, the CEST experiment consists of a selective radio-frequency irradiation of shifted solute protons. These shifted protons exchange with those in water from the bulk solution, until the water signal saturates, thereby enhancing the sensitivity indirectly. Such proton exchange processes have been explored for small molecules (8), protein fragments (9,10), or paramagnetic agents (5,11) and have many potential applications such as for measurement of pH (12–15) or temperature (16,17). Given the size of lipoCEST (hydrodynamic diameter d_H ~200 nm), a major clinical application of such CA is tumor detection, based on specific tumor biomarkers that may be amenable to targeting. Recently, some studies have shown that lipoCEST could be detected when injected into normal tissues or solid tumors (18,19). Even more promising, liposomes encapsulating three different diamagnetic agents were used for multicolor CEST imaging of lymph nodes following intradermal injection (20).

In this study, we examined the feasibility of targeting lipoCEST to a developing brain tumor via an intravenous injection. The integrin $\alpha_v\beta_3$ receptor is expressed strongly during angiogenesis in tumors, but only weakly in normal tissues (21–23). The tripeptide Arginine-Glycine-Aspartic acid or RGD is a known ligand of this receptor and hence a good candidate for targeting tumor angiogenesis (24). We synthesized lipoCEST that were conjugated with RGD on the external surface and evaluated its performance by comparison with a similar, unconjugated lipoCEST (Ctrl-lipoCEST). Mice bearing a brain tumor were injected intravenously with the above

[1]Neurospin, I[2]BM, Commissariat à l'Energie Atomique, Gif-sur-Yvette, France.

[2]Guerbet, Research Division, BP 57400, 95943 Roissy-Charles de Gaulle Cedex, France.

Grant sponsor: Iseult/Inumac French-German project.

*Correspondence to: Fawzi Boumezbeur, Ph.D., NeuroSpin, I[2]BM, CEA, Centre de Saclay, Bât. 145, 91191 Gif-sur-Yvette Cedex, France. E-mail: fawzi.boumezbeur@cea.fr

Received 27 September 2011; revised 25 January 2012; accepted 25 January 2012.

DOI 10.1002/mrm.24217

Published online 29 February 2012 in Wiley Online Library (wileyonlinelibrary.com).

lipoCEST and in vivo MR imaging was performed on anaesthetized mice. Images obtained were analyzed to evaluate the specificity and sensitivity of using the functionalized lipoCEST for targeted imaging of tumor growth. Further, the imaging results were validated by immunohistochemical staining of the imaged brain tissues.

METHODS

Cell Cultures and Animal Model

All experiments were conducted in strict accordance with the recommendations of the European Community (86/609) and the French National Committee (87/848) for care and use of laboratory animals. Human malignant glioma cell line, U87MG, was purchased from ATCC (Rockville, MD) and cultured in Dulbecco's modified Eagle's medium supplemented with 10% fetal bovine serum, 1% glutamine, and 1% gentamicine. Cultures were incubated in controlled atmosphere at 37°C with 5% CO_2 and passaged two or three times a week. Brain tumors were induced by intracerebral injection of U87MG cells, 1.2×10^5 cells in 2 μL, in athymic, immunodeficient nude mice, NU/NU (Janvier, France). Mice were first anesthetized with a ketamine/xylazine mixture (50/7.5 mg/kg, i.p.) and placed in a stereotactic frame. A 1-mm hole was made on the left side of the skull to allow the passage of a Hamilton syringe to inject U87MG cells. About 2–3 weeks later, when the tumor diameters were between 2 and 5 mm, the mice were taken for MR imaging.

LipoCEST Contrast Agents

LipoCEST, with an average hydrodynamic diameter, d_H of ~170 nm, were synthesized by Guerbet Research (Aulnay-sous-Bois, France) (3). Each lipoCEST nanoparticle consisted of a liposome that encapsulated a complex of thulium(4,7-bis-carboxymethyl-1,4,7,10-tetra aza-cyclododeca-1-yl)-acetic acid, bound to two water molecules. The concentration of total lipids was about 23 mM, verified by calibrating with phosphorus element by inductively coupled plasma atomic emission spectroscopy (ICP-AES) measurement after mineralization, and by high-performance liquid chromatography (HPLC) after dissolution of the liposomes in methanol. The total concentration of Thulium atoms Tm(III) was also determined by ICP-AES after mineralization and was around 13 mM. Based on these measurements, the concentration of Tm(III) complexes entrapped was calculated to be ~250 mM and the nanoparticle concentration in solution, C_n ~48 nM. The liposomal membrane was composed of a mixture of lipids: 1-palmitoyl-2-oleoyl-sn-glycero-3-phosphocholine/1,2-dipalmitoyl-sn-glycero-3-phospho-(1′-rac-glycerol)/cholesterol/1,2-distearoyl-sn-glycero-3-phosphoethanolamine-*N*-[methoxy(polyethylene glycol)-2000 (DSPE-PEG_{2000}) at a molar ratio of 32/5/58/5 (Avanti Polar Lipids). A large amount of cholesterol was introduced to reduce permeability of the fluid membrane formed by the unsaturated phospholipids, 1-palmitoyl-2-oleoyl-sn-glycero-3-phosphocholine. PEGylated phospholipids (5%) were added to limit uptake by the reticuloendothelial system in vivo. Rhodamine-phospholipids (0.1%) was incorporated to visualize lipoCEST by fluorescence imaging (25). A complex of RGD peptide conjugated to the lipid DSPE-PEG_{2000}-NH_2 was added (2%) to lipoCEST to obtain functionalized RGD-lipoCEST. Liposomes were prepared by hydration of a thin lipidic film. Briefly, the lipidic mixtures for the RGD-lipoCEST or the native lipoCEST (control) were dissolved in a mixture of chloroform and methanol and the organic solution was slowly evaporated to remove the solvent until a thin film was formed. The film was then rehydrated at 50°C with a 0.3 M of thulium(4,7-bis-carboxymethyl-1,4,7,10-tetra aza-cyclododeca-1-yl)-acetic acid aqueous solution. The resulting suspension of multilamellar vesicles was extruded (Avanti® Mini Extruder) through polycarbonate filters of progressively decreasing mesh size (10 extrusions per filter): 1μm, 800 nm, 400 nm, and 200 nm. The final suspension of liposomes was purified by size exclusion chromatography (Sephadex G25 PD-10) to remove the non-encapsulated Tm(III) complexes. For each lipoCEST preparation, the saturation power that provided maximum CEST effect in vitro was determined by acquisition of z-spectra with an aliquot (200 μL).

MRI Acquisition

Experiments were performed on a 7 T MRI scanner (Bruker, Germany) using an in-house quadrature ^1H coil of 2.8 cm diameter. Mice were anesthetized using an air/O_2 mix (50:50) and isoflurane (1–3%). Respiration rate was monitored and body temperature was held constant at 37°C using an air heater. A catheter with heparin in 0.9% saline buffer was installed in the lateral tail vein and 200 μL of RGD-lipoCEST or Ctrl-lipoCEST were injected as a slow bolus, over ~1 min. The injected dose was 0.32 nmol/kg body weight of nanoparticles corresponding to 87 μmol of Tm(III) complexes/kg body weight. Twelve mice were assigned to two experimental groups each, to receive an intravenous injection of either RGD-lipoCEST or Ctrl-lipoCEST.

The Bruker "Mapshim" routine was used to achieve a water linewidth of ~20 Hz from a $5 \times 7 \times 8$ mm^3 voxel including most of the brain. The anatomical reference image ($Image_{REF}$) was acquired using a multislice-multiecho (MSME) sequence with the following parameters: repetition time (TR) = 5000 ms, 12 echoes registered separately with first echo time (TE_1) = 8 ms and echo spacing = 8 ms, spatial resolution = $150 \times 150 \times 660$ μm^3, T_{acq} = 6 min, n_{slices} = 10. A relatively long TR was used to ensure that longitudinal magnetization was almost fully relaxed between each repetition. The same sequence was used for CEST imaging with an additional saturation module applied ON ($image_{ON}$) and OFF ($image_{OFF}$) resonance. The saturation module consisted of a train of three 128-ms square pulses leading to a total saturation module duration of 384 ms. The saturation module was repeated each pulse TR/n_{slices} (=500 ms), such that the shifted protons were saturated ~80% of the time. The optimum saturation frequency, δ_{sat}, and power, B_1, were determined experimentally by measuring z-spectra for both the lipoCEST over a range of δ_{sat} values of −20 to +20 ppm and B_1 values of 1–10 μT and were set at the values for which lipoCEST exhibited the stronger CEST effects in vitro. CEST images were acquired before ($t = 0'$) and after ($t = 18'$, $30'$, $42'$, $60'$, $72'$, $84'$, $96'$, $108'$) lipoCEST injection by alternating

positive and negative saturation frequencies. The total acquisition time for a CEST image was 12 min while the average time interval between two CEST images was 13.5 min for each CEST image. The difference was due to the fact that reference images were acquired twice during the 2 h acquisition at $t = 6'$ and $t = 48'$ to check for any variation of the reference signal. Both B_0 and B_1 maps were acquired before experiment using WASSR (26) and double angle method (27), respectively. Additionally, an in vivo z-spectrum was also acquired in the mouse brain cortex to estimate endogenous MT background without lipoCEST.

Data Processing

To maximize the signal-to-noise ratio (SNR), each image was reconstructed as a weighted-sum of echo images, weight being equal to the intrinsic SNR calculated on the reference echo image. Moreover, a Tukey filter apodization was performed on raw data leading to a 20% increase in SNR and a 12% degradation of spatial resolution. The CEST contrast specific to the accumulation of lipoCEST in brain tissue was distinguished from the background MT contrast by calculating the asymmetric magnetization transfer ratio (MTRasym) expressed as:

$$\mathrm{MTRasym} = 100 \times \frac{\mathrm{Image}_{\mathrm{OFF}} - \mathrm{Image}_{\mathrm{ON}}}{\mathrm{Image}_{\mathrm{Ref}}}$$

The average MTRasym values were determined for each mouse from the two groups (RGD- or Ctrl-lipoCEST groups) over two regions-of-interest (ROIs): the "tumor" and the "controlateral" regions, i.e., four experimental subgroups. ROIs encompassing similar number of pixels were manually drawn on $\mathrm{Image}_{\mathrm{Ref}}$. A group analysis of mean MTRasym values measured in both ROIs following injection of either RGD- or Ctrl-lipoCEST was performed. Consequently, in the following sections, mean values of MTRasym are given and their standard deviations reflect the intersubject variability within one subgroup. Another group analysis was performed by averaging data from all time points between the first or second hour of acquisition for the four subgroups. Student's *t* test was performed to compare MTRasym values between ROIs and cohorts.

As defined by Liu et al. (28), the contrast-to-noise ratio (CNR) was calculated as $\mathrm{CNR} = \mathrm{contrast}_{\mathrm{post-pre}}/\left(\sqrt{2}.\Delta\right)$ where $\mathrm{contrast}_{\mathrm{post-pre}}$ was the mean signal for each ROI in the images, obtained by subtracting preinjection CEST image from postinjection CEST images. The noise was calculated by multiplying the standard deviation (Δ) of the air noise area by $\sqrt{2}$.

To evaluate typical time-constants T_{in} for accumulation and T_{out} for wash-out under the four experimental conditions, we chose to fit our averaged time-courses by a simple biexponential function given below:

$$A.\left(1 - e^{\frac{-t}{T_{\mathrm{in}}}}\right).e^{\frac{-t}{T_{\mathrm{out}}}} \qquad [2]$$

Histology and Fluorescence Microscopy

Two animals from each group (RGD- or Ctrl-lipoCEST groups) were sacrificed immediately after the MRI session for histological analysis. One animal from each group was subjected to intracardiac perfusion with physiological saline solution containing 4% paraformaldehyde to completely replace blood, including in the brain (called "perfused"); while the other animal was subjected to intracardiac puncture, which removed blood from major veins and arteries, but not from small capillaries (called "nonperfused"). The brain was recovered from the above animals and immersed successively in different solutions as follows: 24 h in a 4% paraformaldehyde solution for tissues fixation, 12 h in 15% sucrose, and finally 24 h in 30% sucrose solution for cryoprotection. Brain tissues were sectioned using a microtome (Microm HM 560, Thermo Scientific) to obtain 20-μm thick slices encompassing a significant section of the tumor. The slices were allowed to react with a primary $\alpha_v\beta_3$ antibody followed by secondary antibody coupled to fluorescein isothiocyanate (FITC) (Millipore, MA). Fluorescence microscopy was performed on an Axio Observer Z1 microscope (Carl Zeiss MicroImaging GmbH, Germany). Fluorescence images of lipoCEST were acquired at excitation wavelength $\lambda_{\mathrm{excitation}} = 557$ nm and emission wavelength, $\lambda_{\mathrm{emission}} = 571$ nm, appropriate for rhodamine that was included in the lipoCEST. The fluorescence images for visualizing $\alpha_v\beta_3$ were acquired using $\lambda_{\mathrm{excitation}} = 495$ nm and $\lambda_{\mathrm{emission}} = 517$ nm, appropriate for FITC. Finally, as a reference for visualizing the tumor, an adjacent slice was stained with hematoxylin and erythrosine (Sigma-Aldrich, St Louis, MO).

RESULTS

Characterization of LipoCEST and MT Contrast

The unconjugated Ctrl-lipoCEST and the conjugated RGD-lipoCEST were first examined for their CEST behavior in vitro to measure the saturation frequency, δ_{sat}, and power, B_1, at which the lipoCEST exhibited the stronger CEST effects. The water-saturation spectra (z-spectra) (Fig. 1a,b) and the MTRasym (Fig. 1c) were recorded for the two lipoCEST in vitro. Both agents exhibited a strong, specific CEST effect in vitro (~20% for Ctrl-lipoCEST and ~17% for RGD-lipoCEST). Although the z-spectra were slightly different for the two lipoCEST, they attained maximum MTRasym at similar saturation parameters (RGD-lipoCEST: $\delta_{\mathrm{sat}} = 7$ ppm and $B_1 = 7$ μT, Ctrl-lipoCEST: $\delta_{\mathrm{sat}} = 8$ ppm and $B_1 = 7$ μT). The affinity of RGD-lipoCEST was found to be in the subnanomolar range based on a concentration–response curve to measure its half maximal inhibitory concentration IC_{50} (data not shown). Next, to characterize the endogenous MT background in vivo z-spectrum was recorded on the mouse brain cortex (Fig. 1d). The MT effect was rather large and symmetrical (ON: 71.74 ± 0.25%; OFF: 71.64 ± 0.19%) leading to a small MTRasym background of 0.10 ± 0.31% at $\delta_{\mathrm{sat}} = 8$ ppm and $B_1 = 7$ μT. Hence, the saturation frequency and power were set at these values for all in vivo experiments in this study.

In Vivo Detection of LipoCEST

Brain tumors were induced in mice by injection of U87MG cells on the left side of the brain. Once the tumors were 2–5 mm in width, animals were randomly assigned to two groups to receive intravenous injection

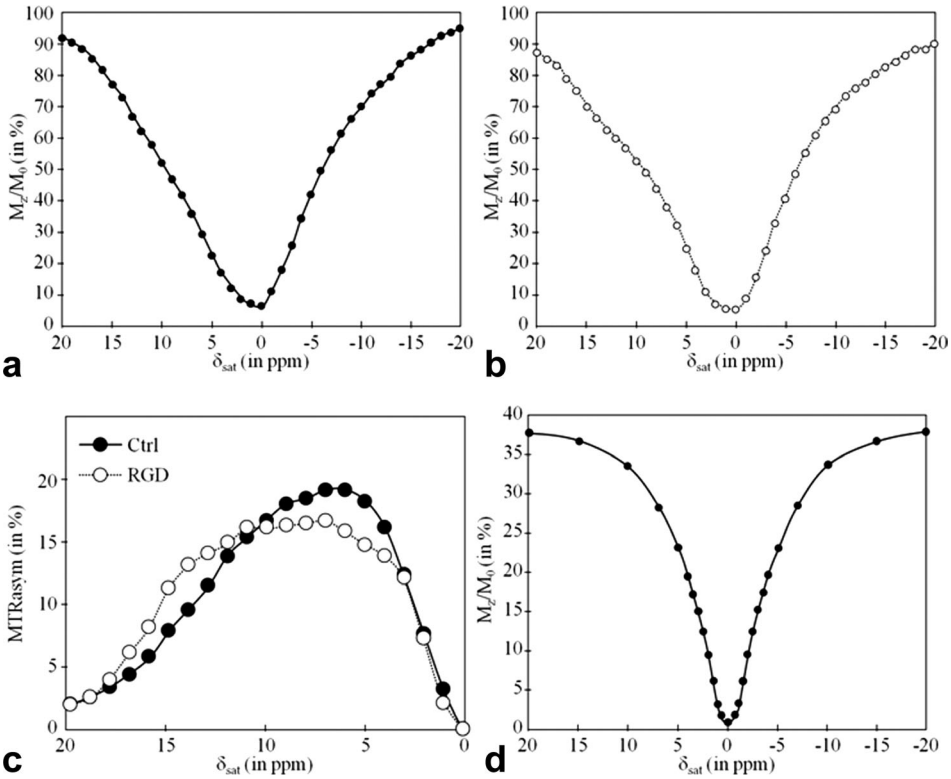

FIG. 1. In vitro CEST effects of lipoCEST. In vitro z-spectrum of (**a**) Ctrl-lipoCEST and (**b**) RGD-lipoCEST; (**c**) in vitro asymmetric z-spectra of Ctrl- and RGD-lipoCEST (filled and empty circles, respectively); (**d**) in vivo z-spectrum of the mouse brain cortex. All z-spectra were acquired using same saturation parameters (B_1 = 7 μT, $\delta_{sat} = -20$ to 20 ppm).

of either RGD- or Ctrl-lipoCEST ($n = 12$ for each group). The mean tumor sizes obtained of the two groups were similar, 3.7 ± 1.1 mm and 4.0 ± 1.0 mm for RGD-lipoCEST and Ctrl-lipoCEST groups, respectively.

Before injecting the lipoCEST, CEST images were acquired to evaluate the MT background in the whole brain of all mice. The mean MTRasym and the standard deviation were calculated for all pixels over the entire cohort: 0.1 ± 0.4% (number of pixels 1.7×10^6). To better illustrate the CEST contrast specific to the presence of lipoCEST, we derived a threshold value from the sum of the mean and SD of the MT background (0.1 + 0.4 = 0.5%) and applied it on all CEST images shown in this paper. The mean value is relatively small, as the saturation conditions ($B_1 = 7$ μT and $\delta_{sat} = 8$ ppm) were not adapted for detection of asymmetric MT contrast. The low MTRasym background also illustrates that the B_0 shimming procedure was effective in limiting any artefactual MTRasym contrast arising from a dissymmetry of the ON- and OFF-resonance saturation frequencies about the water frequency (29). This was further confirmed by the B_0 maps (line width ~20 Hz). Moreover, the B_1 maps established that the saturation was reasonably homogenous over the whole brain ($B_1 = 7.4 \pm 0.5$ μT). This relative inhomogeneity of 7% is typical of a preclinical volumic coil at 7 T (30).

Following intravenous injection of RGD- or Ctrl-lipoCEST, CEST images were acquired over 2 h with an average acquisition time interval of 13.5 min (Fig. 2). ROIs were marked on images on the tumor side and the controlateral side and compared. Notably, for both lipoCEST, a widespread MTRasym contrast was clearly observable especially at shorter times after the injection. Maximum MTRasym values measured in CEST images were as high as 7.9 and 7.5% for RGD- and Ctrl-lipoCEST, respectively. With both lipoCEST, brighter spots were located in the tumor, especially at the periphery. However, the contrast observed following Ctrl-lipoCEST injection (Fig. 2, bottom panel) tended to decrease over the time in both ROIs (within 60 min), whereas it remained high for a comparatively longer period in the tumor ROI following RGD-lipoCEST injection (Fig. 2, top panel).

Sensitivity of LipoCEST Signal In Vivo

Of the 12 mice assigned to RGD- or Ctrl-lipoCEST groups, in two animals from each group, the difference between the tumor and controlateral ROI was not discernible. This could be attributed to the small size of the tumor in these four mice (2.0 mm ≤ tumor diameter ≤ 2.2 mm). Because of the heterogeneity of the CEST contrast in both ROIs, it was difficult to come up with convincing and significant differences for each mouse. Therefore, the mean MTRasym measured in the two ROIs were independently averaged for both cohorts (n = 12 each) at every time point and time-series plots were generated for the four subgroups (Fig. 3). The average MTRasym values for the tumor and controlateral ROIs corresponding to Ctrl-lipoCEST, and the controlateral ROI corresponding to RGD-lipoCEST were statistically similar. The CEST contrast for these three measurements increased to a maximum of 0.95 ± 0.35% during the first hour and decreased to reach an average value of 0.24 ± 0.15% after 108 min. Despite the inhomogeneities of the CEST contrast in the two ROIs (SD varying from 0.15 to 0.38%), the MTRasym in the tumor ROI corresponding to RGD-lipoCEST was significantly higher than both ROIs corresponding to Ctrl-lipoCEST and to the controlateral

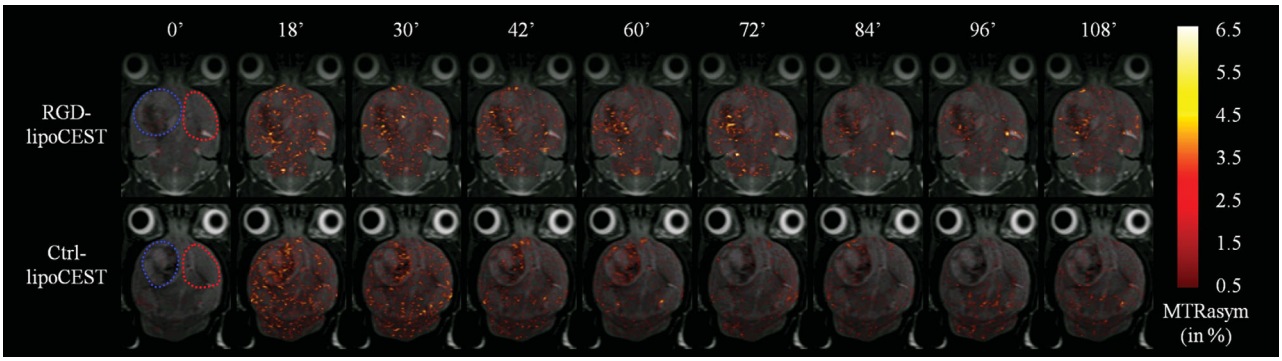

FIG. 2. In vivo CEST images of mouse brain with lipoCEST. Mice bearing U87MG-induced intracerebral tumors (left side) were injected intravenously with either RGD-(top panel) or Ctrl-(bottom panel) lipoCEST. CEST images were acquired before injection of the lipoCEST (0′) and after injection, over a 2-h period with an average interval of 13.5 min. The tumor and controlateral ROIs are delineated by blue and red lines, respectively. These are representative images from one mouse each from the RGD- and Ctrl-lipoCEST groups ($n = 12$ for each group).

ROI corresponding to RGD-lipoCEST (Fig. 3). The maximum CNR between tumor and controlateral ROIs expressed as ($SNR_{tumor} - SNR_{controlateral}$) were 3.2 ± 0.7 and 2.3 ± 0.8 observed at 95 ± 15 min and 27 ± 11 min for the RGD- and Ctrl-lipoCEST, respectively. Thus, the CEST effect of RGD-lipoCEST was stronger and more durable than the Ctrl-lipoCEST. Notably, the maximum CNR values attained after averaging were 2.2 and 1.3 for the RGD- and Ctrl-lipoCEST groups, respectively. These CNR values correspond to probability levels of 90 and 65%, respectively, indicating that the contrast was due to the presence of the lipoCEST (28).

Persistence and Specificity of LipoCEST Signal In Vivo

The above data indicated that the difference in CEST contrast for the two lipoCEST was more pronounced

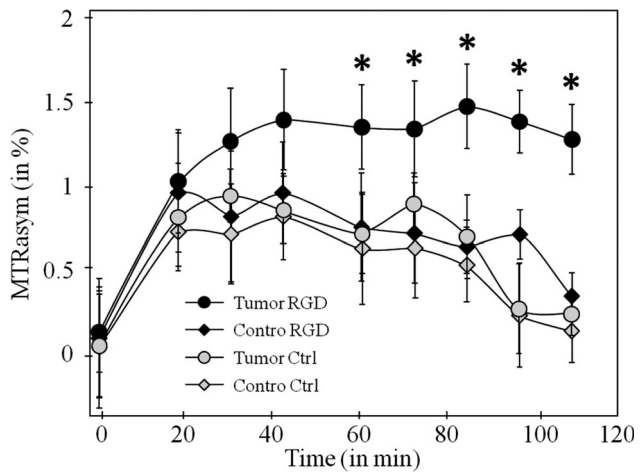

FIG. 3. Time course of lipoCEST signals. Mice bearing U87MG-induced intracerebral tumors were randomly assigned to two groups ($n = 12$ for each group) for intravenous injection with either RGD- or Ctrl-lipoCEST. CEST images were acquired before injection of the lipoCEST (0′) and after injection, over a 2-h period with an average interval of 13.5 min. The tumor and controlateral ROIs were analyzed separately for each group. Mean MTRasym values at each time point over the 2-h acquisition were calculated for the four subgroups and plotted as indicated. *P* values were obtained using a Student's *t* test. The asterisks indicate $P < 0.01$.

beyond 1 h after the intravenous injection. Therefore, the MTRasym values were averaged independently over the first hour and the second hour for the four measurements (Fig. 4a) These calculations confirmed a stronger MTRasym contrast in the tumor region using RGD-lipoCEST during the second hour after injection (1.37 ± 0.23%) compared to its corresponding controlateral region (0.61 ± 0.20%) or either of the regions after Ctrl-lipoCEST injection (0.54 ± 0.25% for tumor region and 0.40 ± 0.27% for controlateral region), with a high significance ($P < 10^{-5}$). It was also noted that the average MTRasym contrast in the tumor region after injection of RGD-lipoCEST was also much higher during the first hour compared to the corresponding controlateral region; however, given the variability, the statistical significance was relatively low ($P = 0.03$).

Averaging of MTRasym values over the first and second hours was also performed for data from single animals shown in Fig. 2. Again, the average MTRasym contrast obtained with RGD-lipoCEST injection appeared to be higher and stayed longer compared to Ctrl-lipoCEST injection, with a better distinction between the tumor and controlateral sides (Fig. 4b).

The time required for accumulation (T_{in}) and washout (T_{out}) of the lipoCEST from the ROI in the brain were determined by applying the averaged time-course data in a simple biexponential function (Fig. 5a,b). The estimated values and the adjustments of averaged time-courses of the two lipoCEST (shown here for RGD-lipoCEST, Fig. 5a) were similar as seen from the high correlation coefficients. For both lipoCEST, the estimated T_{in} values were similar in both ROIs, ranging between 10 and 16 min. In contrast, T_{out} was much longer for the RGD-lipoCEST in the tumor region compared to other three conditions (609 min versus 110–116 min).

Colocalization of RGD-LipoCEST and $\alpha_v\beta_3$ Receptor in Brain Tumors

The brain localization of the IV injected lipoCEST was examined by fluorescence microscopic observation of immunohistochemical staining of the brain slices. The tumor was clearly visible on the optical image after hematoxylin and erythrosine staining and fluorescence

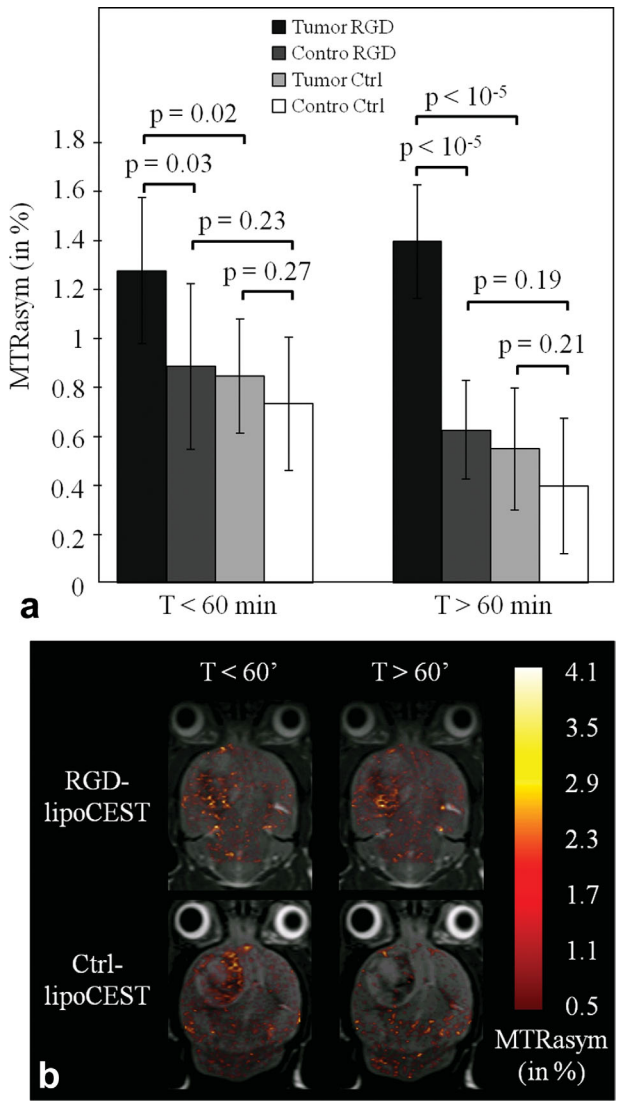

FIG. 4. Persistence of lipoCEST signals. Mice bearing U87MG-induced intracerebral tumors were randomly assigned to two groups ($n = 12$ for each group) for intravenous injection with either RGD- or Ctrl-lipoCEST. CEST images were acquired over a 2-h period with an average interval of 13.5 min. The tumor and contralateral ROIs were analyzed separately for each group. (**a**) Mean MTRasym for pooled data of first ($T < 60$ min) and second hour ($T > 60$ min) of acquisition were calculated for the four subgroups and plotted as indicated. *P* values were obtained using a Student's *t* test. (**b**) Representative images of pooled data of first ($T < 60$ min) and second hour ($T > 60$ min) of acquisition corresponding to one animal from each group (same animals as in Fig. 2).

images were performed in the region delimited by black squares (Fig. 6, first column). The two lipoCEST carried rhodamine, while the RGD target, $\alpha_v\beta_3$, could be visualized with FITC fluorescence. Animals were perfused with saline-paraformaldehyde or nonperfused before recovering the brain tissue. Brain slices from both, perfused and nonperfused animals injected with either RGD- or Ctrl-lipoCEST showed clear and widespread expression of $\alpha_v\beta_3$ in the tumor region, particular at the periphery at the level of blood vessels and capillaries (Fig. 6, second column). In nonperfused brain slices, both lipoCEST appeared to be well distributed, although the coverage and signal intensity of Ctrl-lipoCEST was comparatively lower (Fig. 6, third column, first and third rows). In brain slices from perfused animals, the fluorescent signal of Ctrl-lipoCEST was almost undetectable, but that of RGD-lipoCEST persisted and was similar in strength to the signal observed in the nonperfused animal injected with RGD-lipoCEST (Fig. 6, third column, second and fourth rows). Finally, by merging the images, the RGD-lipoCEST was found to be colocalized with $\alpha_v\beta_3$ receptors in the brain slice from perfused animal (Fig. 6, fourth column, fourth row).

DISCUSSION

The initial in vitro testing of the RGD- and Ctrl-lipoCEST (Fig. 1) showed that both attained maximum MTRasym at similar saturation parameters ($\delta_{sat} = 7$–8 ppm and $B_1 = 7$ μT). These parameters were applied during in vivo imaging. The MT background calculated on all pixel values of all mice ($n = 24$) before lipoCEST injection ($0.1 \pm 0.4\%$) helped to determine the threshold for the MTRasym contrast (0.5%) for an optimal visualization of the lipoCEST. Accordingly, both the intravenously injected lipoCEST could be detected in vivo in the brain in the desired ROIs (Fig. 2). The images acquired over a 2-h period were analyzed individually as well as after averaging the data for a given experimental group (RGD- or Ctrl-lipoCEST) and a given ROI (tumor or controlateral), i.e., for the four experimental conditions (Fig. 3). Data

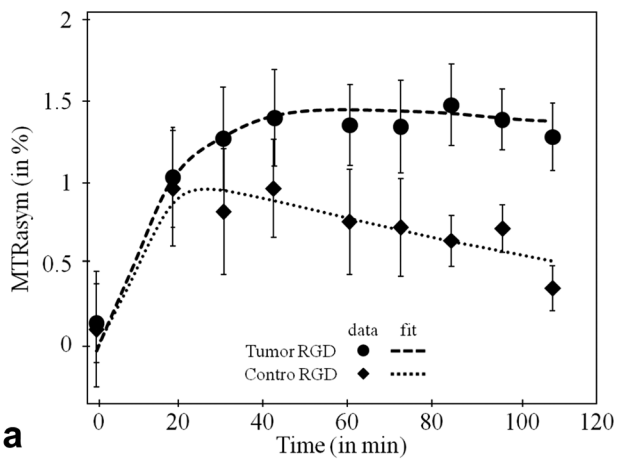

		RGD-lipoCEST T_{in}/T_{out}, min (R^2)	Ctrl-lipoCEST T_{in}/T_{out}, min (R^2)
b	Tumor	16/609 (0.98)	11/116 (0.85)
	Controlateral	12/99 (0.88)	10/115 (0.91)

FIG. 5. Time constants for accumulation of intravenously injected lipoCEST in the brain. Time constants (in min) for the accumulation (T_{in}) and wash-out (T_{out}) of RGD- and Ctrl-lipoCEST from the tumor and controlateral ROIs were determined experimentally and shown here for RGD-lipoCEST (**a**) and calculated using a biexponential function (**b**). Correlation coefficients between the estimated and measured values are given in brackets in (b).

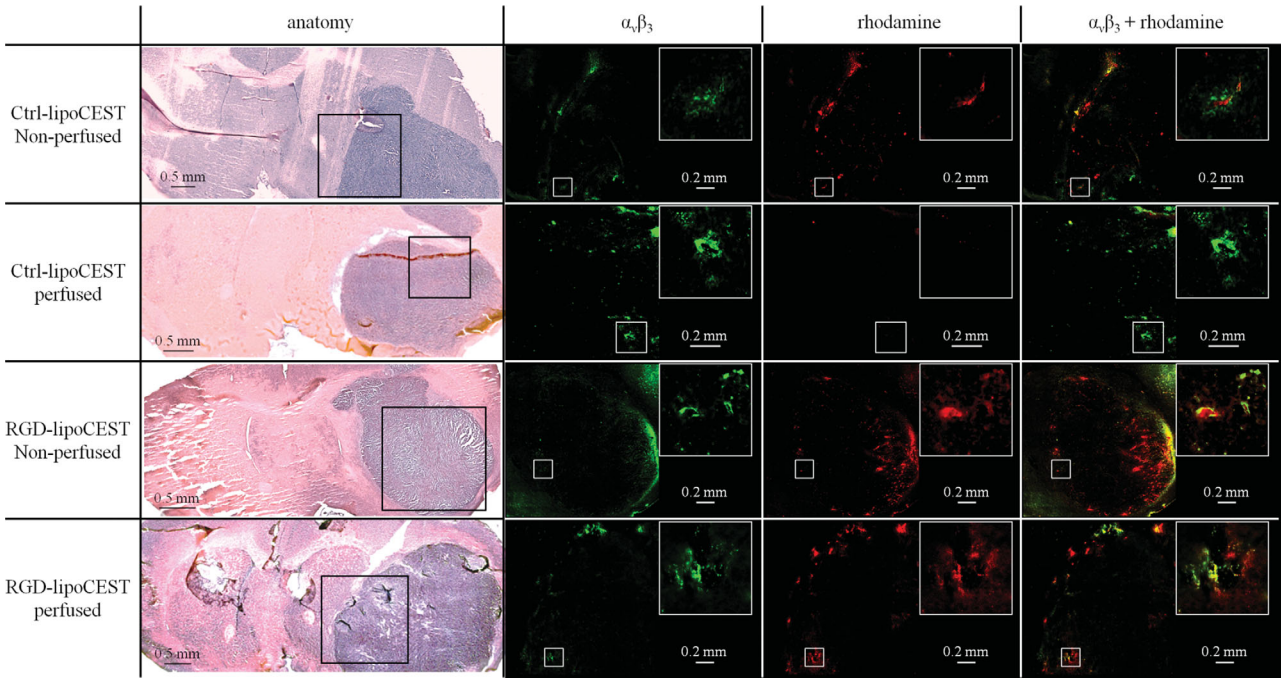

FIG. 6. Colocalization of RGD-lipoCEST with $\alpha_v\beta_3$ receptors in brain tumors. Mice bearing U87MG-induced intracerebral tumors received intravenous injection of either RGD- or Ctrl-lipoCEST. After acquisition of images, animals were sacrificed by intracardiac puncture (nonperfused) or perfused with saline containing 4% paraformaldehyde (perfused). Brain tissue was isolated and sectioned for tumor visualization (hematoxylin and erythrosine staining, first column). The receptors $\alpha_v\beta_3$ were detected using immunohistochemical staining with FITC-labeled secondary antibody (green fluorescence, second column) and observed by fluorescence microscopy in the tumor region. The lipoCEST were tagged with rhodamine (red fluorescence, third column). Colocalization of the two tags was visualized by merging the images (fourth column). For each panel, a selected region of a blood vessel is magnified and presented in the inset.

were also averaged for the first hour or the second hour of imaging (Fig. 4) to compare the persistence of the CEST effect. Further, the averaged data was used to calculate the time constants for accumulation and wash out of the lipoCEST from the brain tissue (Fig. 5). Comparison of the estimated time constants indicated that the two lipoCEST had similar T_{in} values (10–16 min), consistent with the time-constants reported in the literature for nanoparticle CAs of similar diameters (19,21,31). However, the T_{out} was much longer for the RGD-lipoCEST in the tumor region compared to the other three conditions (609 min versus 110–116 min). This very long T_{out} favors the argument that there was accumulation of intact RGD-lipoCEST following specific binding to its biological target. These observations would need to be confirmed by imaging the brain at a much later time point. Taken together, these statistical analyses revealed that compared to Ctrl-lipoCEST, the RGD-lipoCEST exhibited a better contrast, regional specificity (targeting), and persistence of the signal.

Specificity of the interaction of RGD-lipoCEST with the intended target, integrin $\alpha_v\beta_3$ was also confirmed by immunohistochemical staining of brain slices obtained from animals after imaging. The expression of $\alpha_v\beta_3$ was stronger at the periphery of the tumor which is the site for new blood vessels and capillaries during tumor growth, consistent with previous reports (21,22,32). Some amount of nonspecific signals were also seen, which may be because of interaction of the lipoCEST with epithelial cells and/or the eventual degradation of their membrane leading to release of the incorporated rhodamine. To increase the experimental stringency, the brain tissue was perfused with saline to remove blood. Nevertheless, colocalization of the rhodamine signal from RGD-lipoCEST and the FITC signal from anti-$\alpha_v\beta_3$ antibody could be seen even after perfusion of the tissue, lending support to the specificity and strength of the interaction. Thus, we can arguably conclude that the injected RGD-lipoCEST was specifically bound to the targeted biomarker.

The distribution of the injected lipoCEST may be visualized as a four-compartment model: circulating in blood, nonspecifically bound, specifically bound, and degraded. A simple interpretation would be to attribute most of the observed CEST contrast corresponding to Ctrl-lipoCEST or that corresponding to RGD-lipoCEST in the controlateral ROIs, to the lipoCEST nanoparticles circulating very slowly in capillaries or accumulating nonspecifically in the tumor due to enhanced permeability and retention effect. Whereas the persistence of CEST contrast in tumor regions with RGD-lipoCEST would be due to specific binding of lipoCEST to integrin $\alpha_v\beta_3$, which was experimentally confirmed. Finally, the decrease in CEST contrast would be due to either the wash-out or the degradation of the lipoCEST. Such degradation of liposome-based CA may be mediated by macrophages or due to cell entrapment followed by the "quenching" of the CEST contrast as reported earlier (19).

In the future, it would be interesting to increase the time length of observation and to use a faster CEST sequence such as the one proposed by Shah et al. (33) to either increase the temporal resolution or allow for the fast acquisition of z-spectra in vivo. This would permit a better visualization of CEST contrast using a targeted lipoCEST specifically bound to its biological target, as suggest by the results of this study. Moreover, a pixel-by-pixel analysis may help to establish a statistical significance threshold for the CEST effect based on the method proposed by Liu et al. (28). Finally, by application of a model of water exchange processes similar to the one proposed in the literature (34,35), it may be possible to generate maps of lipoCEST concentration, at least semi-quantitative measures, which in turn would allow determination of in vivo kinetics of distribution of the targeted lipoCEST.

The potential toxicity of the lipoCEST described here has yet to be evaluated. However, one can extrapolate this toxicity based on studies previously reported for Gadolinium(III)-complexes. As the composition and stability of Tm(III) and Gd(III) complexes are similar, one can expect the same level of toxicity from these lipoCEST. Moreover, the total dose of Tm(III) complexes administered in this study was 87 μmol/kg body weight, which is lower than the recommended clinical dose of 100 μmol/kg body weight for Gd(III) complexes.

Based on the results of this study and other previous studies, we provide a comparison of the advantages and limitations of using paraCEST or lipoCEST. Several studies have shown that exogenous CEST contrast could be visualized in vivo using paraCEST (15,28,36–40) or lipoCEST (19) and most of them used optimized saturation time and power. Although some previous reports have demonstrated that paraCEST can be detected using nonoptimum saturation power, compatible with in vivo experiments (41), most paraCEST possess high k_{ex} values, which would require rather high B_1 values (up to 30 μT) to reach a maximal CEST effect. Because of the presence of a lipidic membrane that slows down water exchanges between encapsulated paraCEST complexes and bulk water molecules, the overall k_{ex} for lipoCEST complexes is much slower. As stated by Sherry et al. (42,43), the dependency of optimum B_1 (B_{1opt}) on the exchange rate k_{ex} is described by the relationship $k_{ex} = 2\pi \cdot B_{1opt}$. Thus, optimum B_1 values are smaller for lipoCEST compared with most of paraCEST. In this study, we investigated the CEST effect dependency with the saturation power and optimized the MTRasym accordingly. The optimum saturation power for the tested lipoCEST was estimated to be 7 μT (k_{ex} ~1885/s) in vitro at room temperature (data not shown). In future studies, it may be possible to optimize membrane composition to further slow down the water exchange through the lipidic membrane. This would allow for a safer clinical application of CEST-MRI with efficient low saturation power.

As illustrated by the asymmetric z-spectra presented in Fig. 1c, lipoCEST possess a smaller and much variable shifting power compared to most of the paraCEST (42). Thus, the detection of lipoCEST is practically hampered by the endogenous MT background (loss of ~70% of signal at 8 ppm with $B_1 = 7$ μT). One way to limit the interference from endogenous MT effects could be by extending the shifting power by using osmotically shrunken lipoCEST as proposed by Terreno et al. (44). This new generation of lipoCEST is very promising as targeted liposomes have been successfully tested in vitro (45). The 100-pM detection limit estimated in vitro by Aime et al. (2) translates as a 10-fold higher detection limit of ~1 nM in vivo due to endogenous MT. If the number of encapsulated paraCEST complexes is considered (C_i ~250 mM, corresponding to ~6×10^5 paraCEST per nanoparticle), the sensitivity of detection of lipoCEST would be poorer than for a typical paraCEST (~60 μM; (46)), whereas it would be 10^5-fold higher if the number of nanoparticles is considered. As the latter parameter is arguably the most essential for molecular imaging, lipoCEST remains more competitive than paraCEST.

One limitation of lipoCEST is the complexity of their synthesis. As illustrated here, there were some differences between the z-spectra of the Ctrl- and RGD-lipoCEST (Fig. 1a,b, respectively). It is possible that these differences arise from the interference of the RGD peptide with the liposome synthesis. Nevertheless, there is room for improvement in the quality and uniformity of synthesis. Indeed, slight differences in the size distribution of liposomes or internal Tm(III) complexes concentration can impact the maximal attainable MTRasym and the shifting power of lipoCEST.

CONCLUSIONS

High-sensitivity, 7-T MR in vivo imaging of angiogenesis in brain tumor was demonstrated in mice, following intravenous injection of RGD-lipoCEST that was targeted at $\alpha_v\beta_3$ integrin. This is a promising step toward application of lipoCEST for MRI-based molecular imaging of tumors.

ACKNOWLEDGMENTS

The authors thank Gilles Bloch (Commissariat à l'Energie Atomique, Gif-sur-Yvette, France) for his guidance and helpful discussions during this study and Anuradha Alahari for help in editing the manuscript.

REFERENCES

1. Ward KM, Aletras AH, Balaban RS. A new class of contrast agents for MRI based on proton chemical exchange dependent saturation transfer (CEST). J Magn Reson 2000;143:79–87.
2. Aime S, Castelli DD, Terreno E. Highly sensitive MRI chemical exchange saturation transfer agents using liposomes. Angew Chem Int Ed 2005;44:5513–5515.
3. Port M. Contrast agents encapsulating systems for CEST imaging. WO patent 032705; 2006.
4. Terreno E, Castelli DD, Cabella C, Dastru W, Sanino A, Stancanello J, Tei L, Aime S. Paramagnetic liposomes as innovative contrast agents for magnetic resonance (MR) molecular imaging applications. Chem Biodivers 2008;5:1901–1912.
5. Zhang S, Merritt M, Woessner D, Lenkinski R, Sherry A. PARACEST agents: modulating MRI contrast via water proton exchange. Acc Chem Res 2003;36:783–790.
6. Henkelman R, Stanisz G, Graham S. Magnetization transfer in MRI: a review. NMR Biomed 2001;14:57–64.
7. Terreno E, Castelli D, Aime S. Encoding the frequency dependence in MRI contrast media: the emerging class of CEST agents. Contrast Media Mol Imaging 2010;5:78–98.
8. Guivel-Scharen V, Sinnwell T, Wolff SD, Balaban RS. Detection of proton chemical exchange between metabolites and water in biological tissues. J Magn Reson 1998;133:36–45.

9. Goffeney N, Bulte JWM, Duyn J, Bryant LH, van Zijl PCM. Sensitive NMR detection of cationic-polymer-based gene delivery systems using saturation transfer via proton exchange. J Am Chem Soc 2001; 123:8628–8629.
10. Zhou JY, Lal B, Wilson DA, Laterra J, van Zijl PCM. Amide proton transfer (APT) contrast for imaging of brain tumors. Magn Reson Med 2003;50:1120–1126.
11. Zhang SR, Winter P, Wu KC, Sherry AD. A novel europium(III)-based MRI contrast agent. J Am Chem Soc 2001;123:1517–1518.
12. Zhang S, Wu K, Sherry A. A novel pH-sensitive MRI contrast agent. Angew Chem Int Ed 1999;38:3192–3194.
13. Terreno E, Castelli D, Cravotto G, Milone L, Aime S. Ln(III)-DOTAM-GIY complexes: a versatile series to assess the determinants of the efficacy of paramagnetic chemical exchange saturation transfer agents for magnetic resonance imaging applications. Invest Radiol 2004;39: 235–243.
14. Zhou JY, Payen JF, Wilson DA, Traystman RJ, van Zijl PCM. Using the amide proton signals of intracellular proteins and peptides to detect pH effects in MRI. Nat Med 2003;9:1085–1090.
15. Sheth VR, Li Y, Chen LQ, Howison CM, Flask CA, Pagel MD. Measuring in vivo tumor pHe with CEST-FISP MRI. Magn Reson Med 2011, DOI 10.1002/mrm.23038.
16. Zhang S, Malloy C, Sherry A. MRI thermometry based on PARACEST agents. J Am Chem Soc 2005;127:17572–17573.
17. Li A, Wojciechowski F, Suchy M, Jones C, Hudson R, Menon R, Bartha R. A sensitive PARACEST contrast agent for temperature MRI: Eu3+-DOTAM-glycine (Gly)-phenylalanine (Phe). Magn Reson Med 2008;59:374–381.
18. Terreno E, Castelli DD, Milone L, Rollet S, Stancanello J, Violante E, Aime S. First ex-vivo MRI co-localization of two LIPOCEST agents. Contrast Media Mol Imaging 2008;3:38–43.
19. Delli Castelli D, Dastrù W, Terreno E, Cittadino E, Mainini F, Torres E, Spadaro M, Aime S. In vivo MRI multicontrast kinetic analysis of the uptake and intracellular trafficking of paramagnetically labeled liposomes. J Control Release 2010;144:271–279.
20. Liu G, Moake MM, Har-el Y-E, Long CM, Chan KWY, Cardona A, Jamil M, Walczak P, Gilad AA, Sgouros G, van Zijl PCM, Bulte JW, McMahon MT. In vivo multicolor molecular MR imaging using diamagnetic chamical exchange saturation transfer liposomes. Magn Reson Med 2011, DOI 10.1002/mrm.23100.
21. Schmieder A, Winter P, Caruthers S, Harris T, Williams T, Allen J, Lacy E, Zhang H, Scott M, Hu G, Robertson J, Wickline S, Lanza G. Molecular MR imaging of melanoma angiogenesis with alpha(nu)-beta(3)-targeted paramagnetic nanoparticles. Magn Reson Med 2005; 53:621–627.
22. Akers W, Zhang Z, Berezin M, Ye Y, Agee A, Guo K, Fuhrhop R, Wickline S, Lanza G, Achilefu S. Targeting of alpha(v)beta(3)-integrins expressed on tumor tissue and neovasculature using fluorescent small molecules and nanoparticles. Nanomedicine 2010;5:715–726.
23. Eliceiri B, Cheresh D. The role of alpha v integrins during angiogenesis. Mol Med 1998;4:741–750.
24. Schmieder A, Caruthers S, Zhang H, Williams T, Robertson J, Wickline S, Lanza G. Three-dimensional MR mapping of angiogenesis with alpha(5)beta(1)(alpha(v)beta(3))-targeted theranostic nanoparticles in the MDA-MB–435 xenograft mouse model. FASEB J 2008; 22:4179–4189.
25. Park J, Hong K, Carter P, Asgari H, Guo L, Keller G, Wirth C, Shalaby R, Kotts C, Wood W, Papahadjopoulos D, Benz C. Development of anti-P185(HER2) immunoliposomes for cancer-therapy. Proc Natl Acad Sci USA 1995;92:1327–1331.
26. Kim M, Gillen J, Landman B, Zhou J, van Zijl P. Water saturation shift referencing (WASSR) for chemical exchange saturation transfer (CEST) experiments. Magn Reson Med 2009;61:1441–1450.
27. Stollberger R, Wach P. Imaging of the active B–1 field in vivo. Magn Reson Med 1996;35:246–251.
28. Liu G, Ali MM, Yoo B, Griswold MA, Tkach JA, Pagel MD. PARACEST MRI with improved temporal resolution. Magn Reson Med 2009; 61:399–408.
29. Sun P, Farrar C, Sorensen A. Correction for artifacts induced by B(0) and B(1) field inhomogeneities in pH-sensitive chemical exchange saturation transfer (CEST) imaging. Magn Reson Med 2007;58:1207–1215.
30. Doty F, Entzminger G, Kulkarni J, Pamarthy K, Staab J. Radio frequency coil technology for small-animal MRI. NMR Biomed 2007;20: 304–325.
31. Winter P, Caruthers S, Allen J, Cai K, Williams T, Lanza G, Wickline S. Molecular imaging of angiogenic therapy in peripheral vascular disease with alpha(v)beta(3)-integrin-targeted nanoparticles. Magn Reson Med 2010;64:369–376.
32. Eliceiri B, Cheresh D. Role of alpha nu integrins during angiogenesis. Cancer J 2000;6:S245–S249.
33. Shah T, Lu L, Dell K, Pagel M, Griswold M, Flask C. CEST-FISP: a novel technique for rapid chemical exchange saturation transfer MRI at 7 T. Magn Reson Med 2011;65:432–437.
34. Li AX, Hudson RHE, Barrett JW, Jones CK, Pasternak SH, Bartha R. Four-pool modeling of proton exchange processes in biological systems in the presence of MRI-paramagnetic chemical exchange saturation transfer (PARACEST) agents. Magn Reson Med 2008;60:1197–1206.
35. Sun P. Simplified and scalable numerical solution for describing multi-pool chemical exchange saturation transfer (CEST) MRI contrast. J Magn Reson 2010;205:235–241.
36. Jones C, Li A, Suchy M, Hudson R, Menon R, Bartha R. In vivo detection of PARACEST agents with relaxation correction. Magn Reson Med 2010;63:1184–1192.
37. Ali MM, Liu G, Shah T, Flask CA, Pagel MD. Using two chemical exchange saturation transfer magnetic resonance imaging contrast agents for molecular imaging studies. Acc Chem Res 2009;42:915–924.
38. Li A, Suchy M, Li C, Gati J, Meakin S, Hudson R, Menon R, Bartha R. In vivo detection of MRI-PARACEST agents in mouse brain tumors at 9.4 T. Magn Reson Med 2011;66:67–72.
39. Soesbe TC, Togao O, Takahashi M, Sherry AD. SWIFT-CEST: a new MRI method to overcome T(2) shortening caused by PARACEST contrast agents. Magn Reson Med 2011, DOI 10.1002/mrm.23302.
40. Vinogradov E, He H, Lubag A, Balschi JA, Sherry AD, Lenkinski RE. MRI detection of paramagnetic chemical exchange effects in mice kidneys in vivo. Magn Reson Med 2007;58:650–655.
41. Liu G, Li Y, Pagel MD. Design and characterization of a new irreversible responsive PARACEST MRI contrast agent that detects nitric oxide. Magn Reson Med 2007;58:1249–1256.
42. Woessner DE, Zhang SR, Merritt ME, Sherry AD. Numerical solution of the Bloch equations provides insights into the optimum design of PARACEST agents for MRI. Magn Reson Med 2005;53:790–799.
43. Sherry A, Winter P, Wu K. Paramagnetic metal ion-based macrocyclic magnetization transfer contrast agents and method of use. WO 0243775 patent 0243775; 2002.
44. Terreno E, Cabella C, Carrera C, Delli Castelli D, Mazzon R, Rollet S, Stancanello J, Visigalli M, Aime S. From spherical to osmotically shrunken paramagnetic liposomes: an improved generation of LIPOCEST MRI agents with highly shifted water protons. Angew Chem Int Ed Engl 2007;46:966–968.
45. Burdinski D, Pikkemaat JA, Emrullahoglu M, Costantini F, Verboom W, Langereis S, Grüll H, Huskens J. Targeted lipoCEST contrast agents for magnetic resonance imaging: alignment of aspherical liposomes on a capillary surface. Angew Chem Int Ed Engl 2010;49:2227–2229.
46. Wu Y, Zhou Y, Ouari O, Woods M, Zhao P, Soesbe T, Kiefer G, Sherry A. Polymeric PARACEST agents for enhancing MRI contrast sensitivity. J Am Chem Soc 2008;130:13854–13855.